Electronic Supplementary Information

Natures of Optical Absorption Transitions and Excitation Energy Dependent Photostability of Diketopyrrolopyrrole (DPP)-Based Photovoltaic Copolymers

Sebastian Wood,[a] Jessica Wade,[a] Munazza Shahid,[b] Elisa Collado-Fregoso,[b] Donal D. C. Bradley,[a] James R. Durrant,[b] Martin Heeney,[b] Ji-Seon Kim*,[a]

[a]Department of Physics and Centre for Plastic Electronics, Imperial College London, London SW7 2AZ, UK. E-mail: ji-seon.kim@imperial.ac.uk

[b]Department of Chemistry and Centre for Plastic Electronics, Imperial College London, London SW7 2AY, UK

Raman Scattering Cross Sections

Raman spectra for the polymers were measured in chloroform solution in order to obtain absolute Raman scattering cross sections. Figure S1a shows the spectrum measured for chloroform (after subtraction of the photoluminescence background).

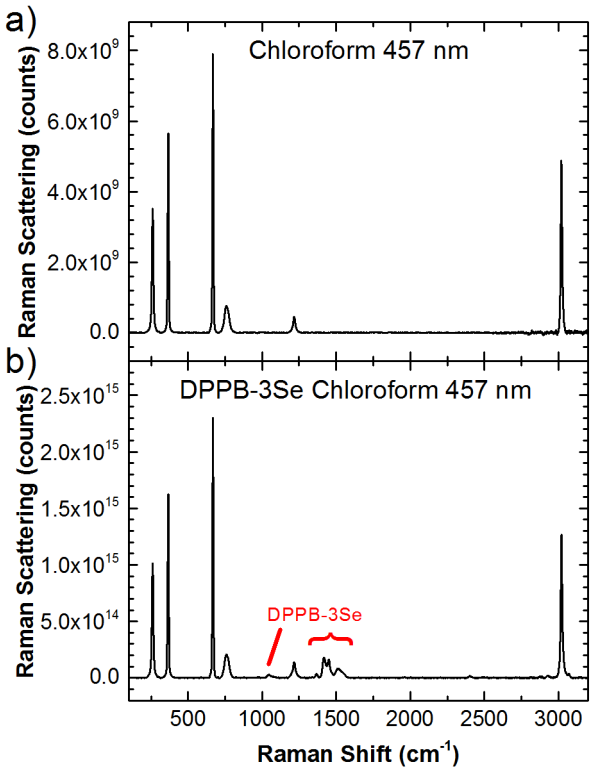

Figure S1. Raman spectra measured with 457 nm excitation for a) chloroform, and b) DPPB-3Se in chloroform solution. Photoluminescence background subtracted.

The chloroform Raman spectrum has clear peaks whose Raman cross sections are well-known. We took reference values quoted for 514.5 nm excitation and adjusted them for the excitation wavelengths we used (457, 488, 514, 633, and 785 nm) using the classical non-resonant dependence for photon counting spectrometry. [1]

$$\beta_j^0 = \beta_j \nu_0 (\nu_0 - \nu_j)^3$$

where:

β_j^0 is the Raman cross section for mode j for excitation at frequency ν_0 [cm^2 molecule^{-1} sr^{-1}]

β_j is the frequency independent Raman cross section for mode j [cm^2 molecule^{-1} sr^{-1}]

ν_0 is the excitation frequency [cm^{-1}]

ν_j is the vibrational frequency of Raman mode j [cm^{-1}]

The measured peak intensities were scaled to the strongest chloroform Raman peak (667 cm^{-1} for calibration) to give calibrated values for the other chloroform peaks from 261 to 3032 cm^{-1}.These values are given in Table S1. By comparing the measured and reference values for the various

chloroform Raman peaks we obtain an indication of the systematic errors in this measurement, which are presented as error bars in Figure S2. We suggest that these errors may arise through small differences in the measurement geometry (though nominally unchanged) and the relatively large discrepancy for the 785 nm excitation is attributed to the poor sensitivity of the CCD in the IR range.

Table S1. Reference and measured values of Raman scattering cross sections for chloroform.[1]

$\times 10^{-30}$ cm^2 molecule^{-1} sr^{-1}	**261 cm^{-1}**	**364 cm^{-1}**	**667 cm^{-1}**	**758 cm^{-1}**	**3032 cm^{-1}**
Reference βj (457 nm)	11.5	10.4	11.1	5.4	8.9
Measured βj (457 nm)	7.7 ± 0.2	9.1 ± 0.5	11.1 ± 0.2	5.0 ± 0.1	8.8 ± 0.1
Reference βj (488 nm)	8.8	8.0	8.5	4.1	6.6
Measured βj (488 nm)	6.0 ± 0.1	7.4 ± 0.1	8.5 ± 0.2	3.3 ± 0.1	7.9 ± 0.2
Reference βj (514 nm)	7.1	6.4	6.9	3.3	5.2
Measured βj (514 nm)	3.9 ± 0.1	5.6 ± 0.1	6.9 ± 0.2	1.7 ± 0.1	6.0 ± 0.2
Reference βj (633 nm)	3.1	2.8	2.9	1.4	2.0
Measured βj (633 nm)	2.9 ± 0.1	2.7 ± 0.1	2.9 ± 0.1	1.5 ± 0.1	2.6 ± 0.1
Reference βj (785 nm)	1.3	1.1	1.2	0.6	0.7
Measured βj (785 nm)	0.93 ± 0.01	1.6 ± 0.1	1.2 ± 0.1	0.15 ± 0.03	0.09 ± 0.01

Raman spectra for the polymers were then measured in chloroform solution with known concentration and show the peaks from the solvent superimposed upon those of the polymer (see Figure S1b) enabling us to use the solvent peaks to calibrate the polymer ones. There are no peaks arising from the chloroform in the 1250-1600 cm^{-1} range of interest for the polymer so the solvent and polymer peaks are readily distinguishable. Cross sections of the various polymer Raman-active modes were measured by fitting the overlapping contributions with pseudo-Voigt peaks and comparing their relative areas with those of the strongest chloroform peak (667 cm^{-1}). In this way (and considering the relative concentrations of solvent and polymer molecules in the sample), absolute Raman cross sections were calculated for the modes of interest.

Figure S2 shows the measured Raman cross sections for the main modes of DPPB-3Se in solution, plotted as a function of excitation wavelength over the range 457 to 785 nm.

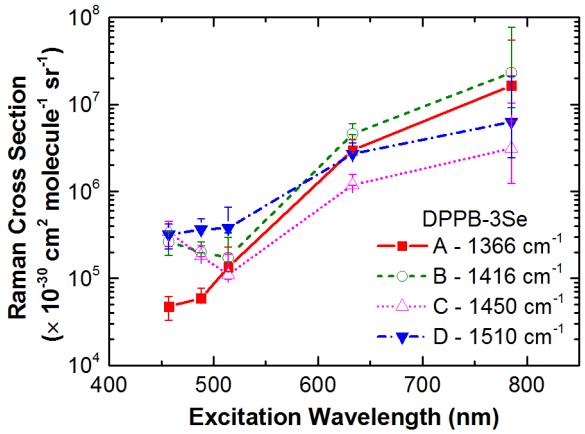

Figure S2. Measured Raman cross sections of the main Raman-active modes in DPPB-3Se as a function of excitation wavelength.

The Raman cross sections measured for the main modes of this polymer are very large (10^{-23} cm^2 $molecule^{-1}$ sr^{-1} at 785 nm, which is comparable with other conjugated molecules such as β-carotene), and show a strong variation over three orders of magnitude within this range of resonant conditions.[1] These factors arise from the high polarizability of the extended conjugated system and the strong extinction coefficient over these wavelengths. All four modes have their largest Raman cross section at 785 nm, corresponding with the strongest absorption peak, showing that all these modes couple to the low energy transition, though not equally strongly. The relative contributions from the different modes in the extreme cases (457 and 785 nm) are discussed in the manuscript, and this comparison with the intermediate wavelengths shows a smooth transition between the two, which supports the hypothesis that this polymer has only two distinct optically-active electronic transitions.

DFT Calculations

Molecular structures were optimised based on symmetric segments of the polymer backbone with truncated alkyl side chains, as illustrated in Figure S3, using the B3LYP hybrid functional and 6-311G(d,p) basis set.[2–6] The decision regarding the length of the polymer segment and truncation of side chains is a compromise since a more complete molecule will provide more accurate results but becomes computationally expensive for diminishing returns. The effects of the branched and straight side chains investigated in this work are therefore not modelled (and unlikely to have a significant impact for an isolated molecule) but this does provide a meaningful comparison for the effect of the sulphur/selenium substitution. The optimised geometry parameters are compared in Table S2.

Table S2. Bond lengths and dihedrals taken from DFT optimised molecular geometries.

Parameter	DPP-3S	DPP-3Se
Dihedral A (°)	2.3	2.1
Dihedral B (°)	12.7	9.9
Bond length A (Å)	1.435	1.433
Bond length B (Å)	1.438	1.432
Se C=C 1 (Å)	1.390	1.388
Se C=C 2 (Å)	1.384	1.381
Se C=C 3 (Å)	1.382	1.380
Se C-C 4 (Å)	1.402	1.404
Se C-C 5 (Å)	1.408	1.409
DPP C=C (Å)	1.398	1.400
DPP central C-C (Å)	1.417	1.416
DPP C-C 6 (Å)	1.445	1.445
DPP C-N 7 (Å)	1.433	1.432
DPP C-N 8 (Å)	1.394	1.395
DPP C-N 9 (Å)	1.462	1.461

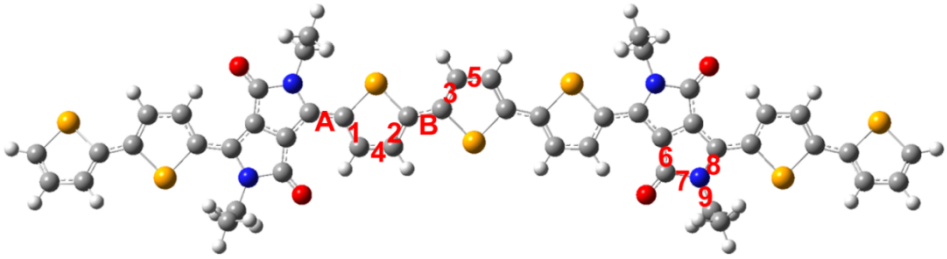

Figure S3. Polymer segment used for DFT calculations.

These results show a high degree of backbone planarity with a larger dihedral for the selenophene-selenophene bond (2.1 °) than for the selenophene-DPP one (9.0 °). The same trend is observed for the thiophene analogue though with slightly larger torsion angles (2.3 and 12.7 °). No significant differences are observed in the bond lengths in the DPP unit, but there are differences in the bond lengths within the selenophene/thiophene units. Specifically, the selenophene substitution, which reduces the dihedral angles, corresponds with a shortening of the interunit C-C bonds. There is also a shortening of the donor ring C=C bonds and a lengthening of the interunit C-C bonds, presumably due to the larger selenium atom donating more electron density into the donor ring.

Time Dependent DFT Calculations

Time dependent DFT (TD-DFT) provides a means for verifying the experimental results presented in the manuscript. Here we use the CAM-B3LYP functional and 6-31G+(d,p) basis set, and consider monomer units of the polymer backbone (computational requirements prohibit larger structures, but CAM-B3LYP tends to reduce the delocalisation of molecular orbitals so should not be strongly affected by additional repeat units).[7–10] The molecular geometry is first optimised in the ground state and then TD-DFT is used to simulate the absorption transitions. Figure S4 shows these results, which agree reasonably well with other published data for DPP-containing molecules[11,12].

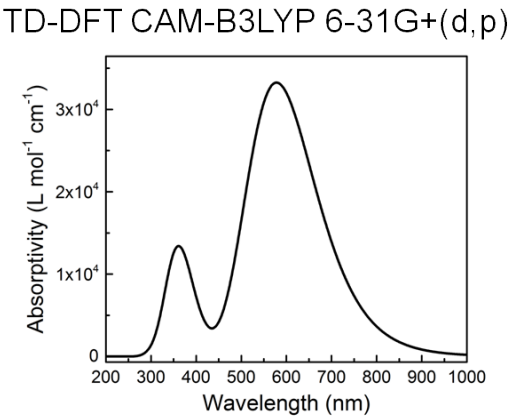

State	Configuration	Oscillator Strength	Transition Energy (eV)	Wavelength (nm)
S_1	133 → 134 (98 %)	0.804	2.3839	520
S_2	132 → 134 (50 %)	0.258	3.4706	357
	133 → 135 (40 %)			

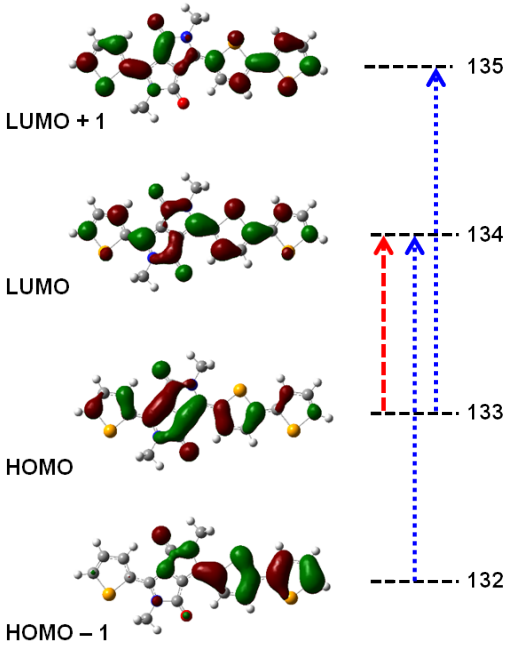

Figure S4. TD-DFT calculation of UV-visible absorption spectrum showing two strong contributions from S_1 and S_2 states. Table shows the contributions to these states from different molecular orbitals, whose electron isodensity surfaces are shown (isovalue is 0.03 atomic units).

Considering the first 6 singlet states of the monomer we identify two absorption transitions with oscillator strengths > 0.1 at 520 nm (0.80) and 357 nm (0.26), which are described in Figure S4. These two absorption bands correspond well with those measured for the polymers described in the manuscript, though the energies are higher in the calculation because we have considered only an isolated monomer. The lowest energy transition corresponds with the HOMO to LUMO transition (orbital 133 to 134), and the isodensity surfaces show that the HOMO is partially localised on the DPP unit, with some density on the adjacent selenophene rings, and the LUMO shows a similar localisation, though perhaps with a slightly increased electron density on the interunit DPP-selenophene bond and the adjacent selenophene units. Significantly, this transition does not have the unambiguous character of an intramolecular charge transfer from the selenophene rings to the DPP unit, in fact the electron density on the DPP ring appears to be reduced in the LUMO. The higher energy absorption band has significant contributions from the HOMO – 1 to LUMO and HOMO to LUMO + 1 transitions. The nature of this transition is less clear because of these two contributions, though we note that the HOMO – 1 molecular orbital is strongly localised on the selenophene ring, so the HOMO – 1 to LUMO transition has a significant coupling to the electron density on the selenophene ring. The LUMO + 1 orbital shows no clear localisation whilst the HOMO is more localised on the DPP unit, hence the HOMO to LUMO + 1 transition is expected to couple to the whole conjugated structure (decrease in electron density on the DPP unit and an increase on the selenophene rings).

Despite the complexity of these results and the need for further work in order to clarify their interpretation, this relatively simple calculation is clearly consistent with the experimental results presented in the manuscript. Specifically, we find that the low energy absorption transition does not correspond with an intramolecular charge transfer from the selenophene to the DPP unit, and does show a strong coupling to the DPP unit. Also there is support for the experimental conclusion that the higher energy absorption transition couples to the whole conjugated structure with a clear contribution from the selenophene rings.

457 nm Photodegradation – Increase of 1450 cm^{-1} Raman peak intensity

Figure 7 in the manuscript shows a relative increase in the intensity of the 1450 cm^{-1} Raman peak relative to the 1416 cm^{-1} peak during photodegradation. This is clear in Figure 7b after subtraction of the fluorescence background, but is not so clear from the raw data in Figure 7a, which shows a strong increase in the background across much of the spectrum. For this reason it is important to demonstrate that the change in the peak intensities is a real effect and that the baseline subtraction is justified.

In fact the large increase in photoluminescence mainly occurs after 200 s of exposure but the increase in 1450 cm^{-1} peak intensity occurs before this. Figure S5 compares the raw spectra measured at 1 s and at 100 s. At these exposure times the increase in the background signal is minimal and the differences in the Raman spectra are already quite clear.

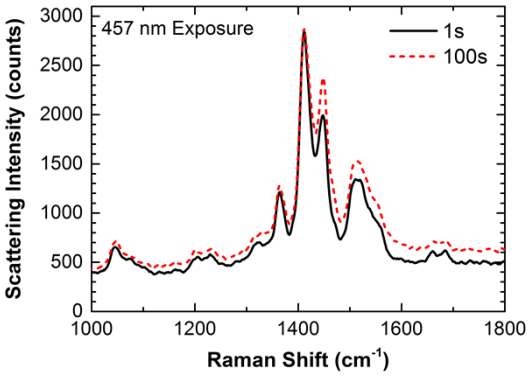

Figure S5. Raw spectra of DPPB-3Se thin film measured after 1 s and after 100 s of exposure to 457 nm illumination.

In Figure 7b a simple linear baseline has been fitted over the range of interest to all the spectra since the large number of features makes it difficult to justify a more complex fitting technique. A linear baseline can also be applied in a robust and repeatable way which minimises the potential for experimenter bias. Alternative baseline subtractions based on polynomials show the same trends and Figure S6 shows the result of an interpolated cubic spline taken from 10 'minima' across the spectrum.

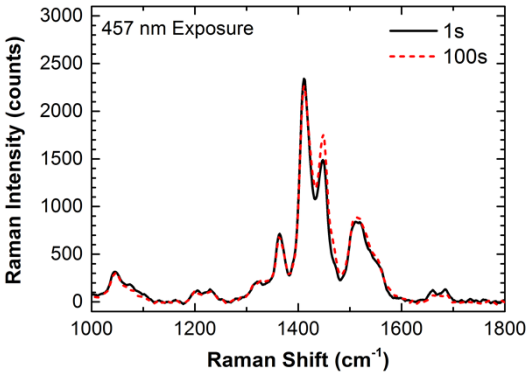

Figure S6. Raman spectra of DPPB-3Se thin film measured after 1 s and after 100 s of exposure to 457 nm illumination using interpolated cubic spline to subtract fluorescence background.

Even without normalising the spectra in Figure S6 it is clear that the 1450 cm^{-1} peak has increased relative to the 1416 cm^{-1} peak. The absolute intensities of these peaks are not robustly measured since the laser spot focussing is sensitive to small movements of the sample, but for consecutive measurements we expect that the absolute scattering intensities may be meaningfully compared. In this case the 1416 cm^{-1} peak intensity is almost identical in both measurements but the 1450 cm^{-1} peak has clearly increased after 100 s of exposure. For this reason we consider that the change in the peak intensity ratio is best interpreted as an increase in the 1450 cm^{-1} scattering rather than a decrease in the other peaks.

The mechanism by which the 457 nm photodegradation causes an increase in the intensity of the 1450 cm^{-1} Raman peak is not yet clear. The plain interpretation of this result is that the degraded molecule has a stronger coupling of the electronic absorption transition at 457 nm to the selenophene C=C

vibrational normal mode. We might expect that breaking the polymer conjugation would result in a quenching of Raman activity, but this does not appear to be the case here. One suggestion might be that the degraded molecule has a stronger absorption coefficient at 457 nm and so the resonant enhancement is greater. Alternatively the increased Raman scattering may come from selenophene units other than the one which is attacked, for example, breaking of one selenophene ring could lead to a redistribution of π-electron density on the neighbouring units, which would affect the Raman activity.

Thermal Degradation

The photodegradation effects described in the manuscript and above may be suspected to have components resulting from thermal degradation, which should also be considered. The high intensity of the optical excitation and its strong absorption by the polymer might be expected to result in localised heating and so the concern is that the degradation might be caused by the high temperature rather than the light exposure. In the manuscript we conclude that the primary observed degradation mechanism is photooxidation of the polymer and it is expected that this process will be aggravated by high temperatures but it is important to establish whether the same effects are observed when the sample is exposed to high temperatures without optical excitation.

Raman spectra were measured for thin film samples at high temperatures (250-425 °C) using a Linkam THMS600 hot-cold cell purged with nitrogen gas. Spectra were measured during heating and the sample was held at each temperature for 5 minutes. Figure S7 shows the Raman spectra of an identical sample measured at temperatures up to 425 °C. These spectra are normalised to the 1416 cm^{-1} peak (except for the 425 °C spectrum measured at 457 nm, which lacks this peak).

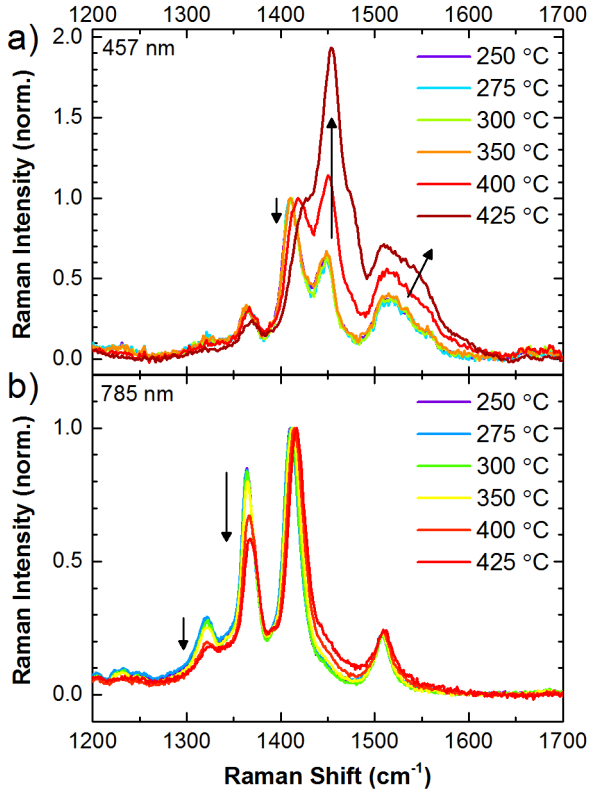

Figure S7. Raman spectra of DPPB-3Se thin film measured at temperatures from 250-425 °C.

As the temperature of the sample is increased the Raman spectrum measured at 457 nm (Figure S7a) shows minimal change up to 350 °C. Above this temperature there is a loss of the 1416 cm^{-1} peak resulting in a relative growth of the 1450 cm^{-1} peak and a slight broadening of the 1515-1550 cm^{-1} band, and a new shoulder appearing at 1475 cm^{-1}. These changes are similar to those described in Figure 7 as the result of photodegradation. However, when we consider the 785 nm Raman spectra for the same temperature range (Figure S7b) we observe distinctive features of this thermal degradation. Here the spectrum shows a steady decrease in the relative intensities of the peaks at 1321 and 1364 cm^{-1} over the temperature range 275-425 °C, which is not observed for photodegradation (Figure 8).

By comparing the 785 nm spectra (Figure 8 and Figure S7b) we can conclude that thermal degradation does not occur during the photoexcitation experiment with 785 nm excitation. Photodegradation with 457 nm excitation clearly has a similar impact to thermal degradation above 350 °C, but if there is no thermal degradation in the 785 nm excitation case (which has the same intensity, but longer exposure time and is absorbed more strongly by the sample), then we do not expect it for 457 nm excitation either.

Polymer Synthesis

General: All solvents and chemicals, were purchased from Sigma-Aldrich and used without further purification. Microwave reactions were performed in a Biotage initiator V 2.3 in constant temperature mode. Nuclear magnetic resonance (NMR) spectra were recorded on Bruker AV-400 (400 MHz) spectrometers in chloroform-*d* solutions. Number-average (M_n) and weight-average (M_w) molecular weights were determined with an Agilent Technologies 1200 series GPC in chlorobenzene at 80°C using two PL mixed B columns in series, and calibrated against narrow polydispersity polystyrene standards.

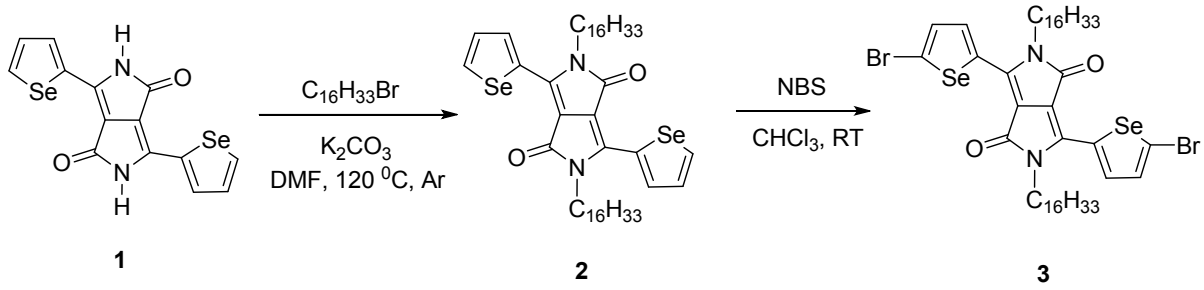

1 **2** **3**

2,5-Di(2-hexadecyl)-3,6-bis-(selenophenyl)-1,4-diketopyrrolo[3,4-c]pyrrole (2)

3,6-Bis-(selenophenyl)-1,4-diketopyrrolo[3,4-c]pyrrole[13] (2.9 g, 7.35 mmol), anhydrous potassium carbonate (4.57 g, 33.07 mmol) and 18-crown- 6 (~30 mg) in dry DMF (60 mL) were heated to 100 °C. 1-Bromohexadecane (8.98 g, 29.4 mmol) was added slowly to the mixture and reaction stirred at 120 °C. After 20 h the reaction mixture was cooled, poured into ice-water (200 mL) and extracted with chloroform (3 x 100 mL).The combined extracts were washed with water and brine and dried ($MgSO_4$). The solvent was then removed under reduced pressure and the crude product was purified by column chromatography on silica (eluent: chloroform: hexane 3:7 to 1:2; 1 % added triethylamine) to give **2** as a deep red solid (3.3 g, 53 %).

^{1}H NMR ($CDCl_3$) δ (ppm): 8.87 (dd excl. Se satellites, J = 1.0 Hz, J = 4.1 Hz, 2H), 8.43 (dd, J = 1.0 Hz, J = 5.6 Hz, 2H), 7.52 (dd, J = 4.10 Hz, J = 5.6 Hz, 2H), 4.08 (t, J = 7.7 Hz, 4H), 1.76 (m, 4H),

1.27 (m, 52H), 0.87 (t, 6H) . ^{13}C NMR ($CDCl_3$) δ (ppm): 161.87, 142.15, 136.88, 136.34, 134.04, 108.58, 46.15, 37.65, 31.92, 31.86, 31.21, 29.99, 29.62, 29.54, 29.48, 29.34, 29.27, 26.19, 22.65, 14.10, ^{77}Se NMR ($CDCl_3$) δ (ppm): 645.86 (ddd, J = 5.2 Hz, J = 7.6 Hz, J = 48.7 Hz). MS (ESI) : *m/z* 844 $[M+H]^+$

2,5-Di(2-hexadecyl)-3,6-bis-(5-bromoselenophenyl)-1,4-diketopyrrolo[3,4-c]pyrrole (3)

To a stirred solution of **2** (1.09 g, 1.3 mmol) in chloroform (90 mL) under argon atmosphere, *N*-bromosuccinimide (0.51 g, 2.86 mmol) was added in small portions and the mixture stirred overnight at room temperature. The reaction mixture was poured into methanol (300 mL) and kept in refrigerator overnight. The resulting precipitates were filtered and washed with hot distilled water and methanol. The crude product was further purified by column chromatography on silica (eluent: chloroform: hexane 2:1) to obtain **3** as a dark purple solid (1.0 g, 78 %)

^{1}H NMR ($CDCl_3$) δ (ppm): 8.49 (d excl. Se satellites, J = 4.4 Hz, 2H), 7.45 (d, J = 4.42 Hz, 2H), 3.96 (t, J = 7.7 Hz, 4H), 1.73 (m, 4H), 1.28 (m, 52H), 0.90 (t, 6H). ^{13}C NMR ($CDCl_3$) δ (ppm): 161.52, 140.88, 136.05, 135.61, 134.23, 123.69, 108.27, 50.87, 46.18, 37.63, 31.78, 31.56, 31.17, 29.97, 29.79, 29.54, 29.43, 29.36, 26.14, 22.69, 14.12, ^{77}Se NMR ($CDCl_3$) δ (ppm): 707.75 (dd, J = 1.4 Hz, J = 2.4 Hz). MS (ESI): *m/z* 1001.7 (M^+)

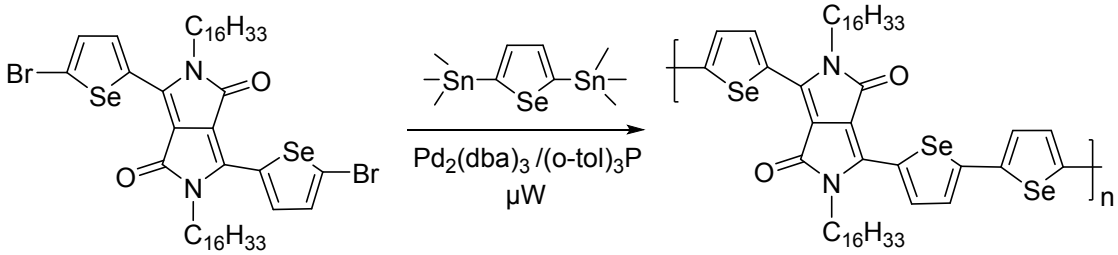

(Poly[[2,5-bis(2-hexadecyl)-2,3,5,6-tetrahydro-3,6-dioxopyrrolo[3,4-c]pyrrole-1,4-diyl]- alt – [[2,2'-(2,5-selenophene)bis-selenophene]-5,5'-diyl]])

To a 2 mL microwave vial was added 2,5-di(2-hexadecyl)-3,6-bis-(5-bromoselenophenyl)-1,4-diketopyrrolo[3,4-c]pyrrole 4 (0.17 g, 0.17 mmol), 2,5-bis(trimethylstannyl)selenophene (0.082 g, 0.17 mmol). Chlorobenzene (1 mL) was added and the solution degassed before addition of $Pd_2(dba)_3$ (2.5 mg, 2.7 μmol, 1.5 mol%) and P(*o*-Tol)$_3$ (3.3 mg, 10 μmol, 6 mol%). The reaction mixture was further degassed and subsequently sealed. The vial was heated in a microwave reactor at 100 °C (2 min), 140 °C (2 min), 170 °C (2 min) and 200 °C (30 min). After cooling to room temperature, the mixture was added to vigorously stirred methanol (200 mL), filtered and washed with methanol (2 x 25 mL). The polymeric material was purified by Soxhlet extraction with acetone (24 h) and hexane (24 h). After cooling to room temperature, the polymer was dried in vacuo and dissolved in chloroform by heating and stirring. To the chloroform extract was added an aqueous solution of sodium diethyldithiocarbamate (~1 g/100mL) and the mixture was heated to 60 °C with vigorous stirring for 2 h. After cooling to room temperature, the layers were separated and the organic fraction was washed with water (2 x 250 mL), and concentrated under reduced pressure. The resulting residue was dissolved in a minimum amount of chloroform and added dropwise to vigorously stirred methanol (250 mL). The precipitates were filtered over a 4.5 μm PTFE filter and dried under vacuum to afford the desired polymer (112 mg, 68 %). GPC (chlorobenzene, 80 °C): M_n = 33,000 g/mol, M_w = 48,000 g/mol.

References

1 R. L. McCreery, *Raman Spectroscopy for Chemical Analysis*, John Wiley & Sons, New York, 2000.

2 A. D. Becke, *J. Chem. Phys.*, 1993, **98**, 5648–5652.

3 P. J. Stephens, F. J. Devlin, C. F. Chabalowski and M. J. Frisch, *J. Phys. Chem.*, 1994, **98**, 11623–11627.

4 A. D. McLean and G. S. Chandler, *J. Chem. Phys.*, 1980, **72**, 5639–5648.

5 R. Krishnan, J. S. Binkley, R. Seeger and J. A. Pople, *J. Chem. Phys.*, 1980, **72**, 650–654.

6 L. A. Curtiss, M. P. McGrath, J.-P. Blaudeau, N. E. Davis, R. C. Binning and L. Radom, *J. Chem. Phys.*, 1995, **103**, 6104.

7 S. Few, J. M. Frost, J. Kirkpatrick and J. Nelson, *J. Phys. Chem. C*, 2014, **118**, 8253.

8 M. E. Reish, S. Nam, W. Lee, H. Y. Woo and K. C. Gordon, *J. Phys. Chem. C*, 2012, **116**, 21255–21266.

9 T. Yanai, D. P. Tew and N. C. Handy, *Chem. Phys. Lett.*, 2004, **393**, 51–57.

10 N. Banerji, E. Gagnon, P.-Y. Morgantini, S. Valouch, A. R. Mohebbi, J.-H. Seo, M. Leclerc and A. J. Heeger, *J. Phys. Chem. C*, 2012, **116**, 11456–11469.

11 Y. Li, J. Cui, J. Zhao, J. Liu, P. Song and F. Ma, *Sci. World J.*, 2013, 890215.

12 D. Moghe, G. K. Dutta, S. Patil and S. Guha, *Phys. Chem. Chem. Phys.*, 2014, **16**, 4291.

13 M. Shahid, T. McCarthy-Ward, J. Labram, S. Rossbauer, E. B. Domingo, S. E. Watkins, N. Stingelin, T. D. Anthopoulos and M. Heeney, *Chem. Sci.*, 2012, **3**, 181.